Contemporary Mathematics
https://ojs.wiserpub.com/index.php/CM/

Research Article

Adaptive Fourier Decomposition in Epidemic Analysis: Precision Evaluation of Vietnam's Policies

Xin Bai[1,2,†], Xuanfeng Li[1,2,†], Yiping Li[3], Kai Guo[4], Kai Gu[5], Chitin Hon[1,2*]

[1] Faculty of Innovation Engineering, Macau University of Science and Technology, Taipa, Macau SAR, 999078, China
[2] Institute of Systems Engineering, Macau University of Science and Technology, Macau SAR, 999078, China
[3] Faculty of Humanities and Arts, Macau University of Science and Technology, Taipa, Macau SAR, 999078, China
[4] Faculty of Information Engineering, Zhongnan University of Economics and Law, Wuhan, 430073, China
[5] College of Foreign Studies, Faculty of Social Science, Nanjing Agricultural University, Nanjing, 210095, China
[†] These authors contributed equally to this work.
E-mail: cthon@must.edu.mo

Received: 14 May 2025; **Revised:** 10 July 2025; **Accepted:** 22 July 2025

Abstract: Since the outbreak of the novel Coronavirus Disease 2019 (COVID-19) in late 2019, the epidemic has significantly impacted social stability, the economy, and public health. Traditional epidemiological models like SI, SIS, SIR, SIRS, SEIR, and SEAIR are commonly used to analyze epidemic spread but face limitations due to assumptions of population homogeneity, difficulties in capturing non-linear and non-stationary dynamics, and challenges in representing spatial-temporal variations. This study introduces Adaptive Fourier Decomposition (AFD), an innovative method that improves data decomposition accuracy by addressing non-stationary signal characteristics and adapting to the time-varying nature of epidemic data. Using COVID-19 infection data from Vietnamese cities, we analyze transmission trends and evaluate the government's policies. The results show that AFD captures COVID-19 transmission dynamics more accurately than traditional methods, underscoring the importance of advanced mathematical tools in public health modeling and the necessity of timely, precise policy measures to control epidemics.

Keywords: Adaptive Fourier Decomposition (AFD), COVID-19, vietnam epidemic, epidemic prevention policies

MSC: 42A38

Abbreviation

AFD	Adaptive Fourier Decomposition
WHO	World Health Organization
EMD	Empirical Mode Decomposition
VMD	Variational Mode Decomposition
SEAIR	Susceptible-Exposed-Asymptomatic-Infected-Recovered

DOI: https://doi.org/10.37256/cm.6420257234

1. Introduction

Since the first outbreak of the novel coronavirus causing COVID-19 in late 2019, governments have taken a series of policy measures to prevent the further spread of the virus, including city lockdowns, movement restrictions, social quarantines, face mask mandates, and mass testing and vaccination [1]. However, due to virus mutation and the varying effectiveness of anti-epidemic measures, the number of infected persons in different places shows different trends, posing more significant difficulties in assessing the effectiveness of anti-epidemic policies and analyzing future epidemics. Changes in the number of people infected with the new coronavirus reflect the severity of the epidemic and the speed of its spread.

At the beginning of the epidemic, the Vietnamese government adopted a series of strict preventive measures to control the initial spread of the epidemic successfully, and the government's timely preventive measures played a crucial role in stopping the epidemic [2]. However, with the gradual resumption of international traffic and the mutation of the virus, especially with the emergence of the Delta mutant strain, Vietnam has also seen several outbreaks rebound, with fluctuating trends in the number of infected people [3].

Against the backdrop of this global health crisis, the development of the outbreak and the effectiveness of prevention and control in Vietnam has become a critical case study for research [4]. The study by the team of Thuong Vu Nguyen, a scholar at the Pasteur Institute in Ho Chi Minh, presents the status of the COVID-19 outbreak in Vietnam, the primary response successes, the factors that prompted the implementation of specific public health actions, and the impacts of these actions. Developing a new coronavirus outbreak is not just a problem for one country or region but a common challenge for all humankind [5]. By analyzing the development of the epidemic and changes in the number of infected people in Vietnam and globally, we can better understand the pattern of virus transmission and the effectiveness of anti-epidemic policies and provide a scientific basis and reference experience for future public health crisis response and epidemic prevention and control [6–8].

The origins and development of epidemic transmission models date back hundreds of years, and with advances in mathematics and biology, these models have become an essential tools in public health [9–11]. Classical epidemic models are currently available: SI [12], SIS [13], SIR [14, 15], SIRS [16], SEIR [17], and SEAIR [18]. In epidemiological modeling analyses, the number of cases, the rate of state transitions, and the effectiveness of preventive and control measures are usually first considered as time-domain signals. Time-domain signals reflect how signals change over time and directly show how a variable or variables change over time. However, we need a way to do mathematical modeling of data, such as the number of new infections, which is non-linear and has frequency domain properties. Commonly used time domain analysis decompositions such as Empirical Mode Decomposition (EMD) [19], Variational Mode Decomposition (VMD) [20]; Dong et al. analyzed epidemic spread using EMD [21]. However, in COVID-19 analyses, boundary effects may arise when dealing with signal boundaries, leading to inaccurate decomposition results, especially in epidemic data. To better analyze the daily data of newly infected persons, Qian et al. studied and analyzed the AFD method [19, 20], which makes up for the shortcomings of the EMD decomposition method, and this paper will also argue that the AFD is more suitable for analyzing the number of newly infected persons per day in the COVID-19 and the trend of development.

While this study focuses on Vietnam's domestic policy effectiveness, we acknowledge that international factors may influence epidemic dynamics. However, Vietnam's unique characteristics during the study period justify this domestic-focused approach. Vietnam implemented comprehensive border controls and international travel restrictions early in the pandemic, creating a relatively isolated epidemiological environment. The country maintained consistent domestic data reporting standards throughout the study period, and the temporal separation between domestic policy waves enables clear analytical phases for intervention assessment. Future research incorporating cross-border policy influences would require standardized international data protocols and advanced network analysis methods beyond the scope of this study.

2. Methods

2.1 *AFD*

Specifically designed to analyze non-stationary signals whose statistical properties vary temporally, AFD addresses fundamental limitations of traditional Fourier analysis methods that assume fixed frequency components [23]. This adaptive decomposition capability proves particularly valuable for epidemic data analysis, where transmission dynamics exhibit rapid temporal variations due to policy interventions and behavioral changes.

AFD demonstrates superior capacity for handling non-stationary signals through its foundation in Hardy space theory [24], providing mathematical rigor and theoretical guarantees for signal decomposition that empirical methods like EMD lack [25, 26]. The methodology incorporates adaptive parameter optimization via maximal selection principles, substantially reducing subjective bias inherent in manual parameter tuning required by VMD and similar approaches [27]. Furthermore, AFD exhibits superior boundary effect resistance essential for finite time series analysis, maintaining completeness and orthogonality properties without significant edge artifacts that compromise traditional Fourier analysis [28]. Notwithstanding these advantages, AFD presents certain limitations requiring consideration. Computational complexity scales significantly with signal length, requiring O (MN^2) operations that may limit practical applicability for large datasets [29]. The method necessitates complex-valued analysis involving Blaschke products and rational orthogonal systems, creating analytical challenges compared to real-valued alternatives [22]. Performance dependency on signal-to-noise ratio results in diminished effectiveness under low SNR conditions commonly encountered in real-world applications [30]. Additionally, AFD's greedy algorithm nature may lead to over-decomposition of smooth signals, generating unnecessary mono-components that obscure signal interpretation and increase computational burden [31].

The Takenaka-Malmquist system uses $\{E_m\}_{m=1}^{\infty}$ as the basic element for AFD:

$$E_m(e^{jt}) = \frac{\sqrt{1-|a_m|^2}}{1-\bar{a}_m e^{jt}} \prod_{h=1}^{m-1} \frac{e^{jt}-a_h}{1-\bar{a}_h e^{jt}}, \tag{1}$$

where $a_{\mathrm{m}} \in \mathrm{D},\ \mathrm{D} \subseteq \mathrm{C},\ \mathrm{m} = 1,\ 2,\ \cdots,\ \mathrm{C}$ represents the complex plane [22]. Given $E_m\ (e^{jt})$ and a_{m}, the primary task of AFD is to find such an array $\{a_1,\ a_2,\ \cdots,\ a_{\mathrm{m}}\}$, ensuring all decomposed components only contain phase derivatives with high decomposition efficiency and physical significance.

In the AFD algorithm, to swiftly identify the energy relationship, all single components are extracted sequentially from high to low energy, reducing the remainder $G_m{}'$s and defining $R_{m-1}{}'$s along with the corresponding standard remainder [32]:

$$G_m(e^{jt}) = R_{m-1}(e^{jt}) \prod_{p=1}^{m-1} \frac{1-\bar{a}_p e^{jt}}{e^{jt}-a_p}, \tag{2}$$

The signal can be represented by a reduced remainder $G_m{}'$s:

$$G(t) = \sum_{m=1}^{N} \langle G_m,\ e_{\{a_m\}} \rangle E_m(e^{jt}) + G_{N+1}(e^{jt}) \prod_{m=1}^{N} \frac{e^{jt}-a_m}{1-\bar{a}_p e^{jt}}, \tag{3}$$

where $e_{\{a_m\}}(e^{jt})$ is called the evaluator, and a_m forms a dictionary of complex Hardy Spaces $H^2\ (D)$.

$$e_{\{a_m\}}(e^{jt}) = \frac{\sqrt{1-|a_m|^2}}{1-\bar{a}_m e^{jt}}, \tag{4}$$

The complex Hardy space in the unit circle D is defined [33] as follows:

$$H^2(D)=\left\{f{:}D\to\mathbb{C}{:}f \text{ is holomorphic, and } \|f\|_2^2\overset{\Delta}{=}\sup_{0\le r<1}\int_0^{2\pi}|f(re^{it})|^2dt<\infty\right\}, \tag{5}$$

According to the equation above, $G(t)$ can be calculated by [22]:

$$\|G(t)\|^2=\sum_{m=1}^{N}\left|\langle G_m,\ e_{\{a_m\}}\rangle\right|^2+\|G_{N+1}(e^{jt})\|^2, \tag{6}$$

To minimize the energy of the standard remainder $\|G_{N+1}(e^{jt})\|^2$, find the maximum value of a_m using the maximum projection principle [32].

$$a_m=\arg\max\left\{\left|\langle G_m,\ e_{\{a_m\}}\rangle\right|^2:a_m\in D\right\}, \tag{7}$$

From the algorithm's point of view, there are apparent differences between the AFD method and the traditional decomposition method. AFD decomposes the signal according to its energy distribution and is suitable for separating signals with overlapping frequencies [25].

2.2 *Component reconstruction of decomposition results*

AFD has various variant modes, including core AFD, unwinding AFD, cyclic AFD, and random AFD [22, 26, 34–36], which should be applied to solve real-world problems, as demonstrated in [35, 36]. When decomposing large-scale data signals, multiple layers of decomposition results are expected to be set up to ensure thorough decomposition [37, 38]. This inevitably leads to redundant data in the signal decomposition. By reconstructing and merging parts of the decomposition results, the risk of data errors can be reduced, and data reliability can be improved. Therefore, we attempt to reconstruct the decomposition results:

$$F_n=\sum_{q=1}^{n}C_qE_q\left(e^{jt}\right), \tag{8}$$

where $E_q(e^{jt})$

$$=\frac{\sqrt{1-\left|a_q\right|^2}}{1-\bar{a}_qe^{jt}}\prod_{h=1}^{q-1}\frac{e^{jt}-a_h}{1-\bar{a}_he^{jt}}, \tag{9}$$

Algorithm 1 Basic AFD Algorithm

Require: Signal $s(t)$; Sampling points $t_k=2\pi\Delta k$ where $\Delta=\dfrac{1}{M}$, $t_k\in[0,\ 2\pi]$

Ensure: Decomposition components $\{e_{\{a_n\}}\}_{n=1}^{M}$

1: Initialize parameters:

2: $a_1\leftarrow 0, N\leftarrow 1$

3: $G(t)\leftarrow G_1(t)\leftarrow s(t)$

4: Compute initial basis:

5: $e_{\{a_1\}} \leftarrow \dfrac{\sqrt{1-|a_1|^2}}{1-\overline{a}_1 e^{jt}}$

6: $E_1 \leftarrow e_{\{a_1\}}$

7: Update residual component:

8: $G_2 \leftarrow \left(G(t) - \langle G_1, e_{\{a_1\}}\rangle e_{\{a_1\}}\right) \dfrac{1-\overline{a}_1 e^{jt}}{e^{jt}-a_1}$

9: Optimize parameter selection:

10: $a_2 \leftarrow \underset{a_2 \in D}{\arg\max} \left\{ \left| \langle G_2, \dfrac{\sqrt{1-|a_2|^2}}{1-\overline{a}_2 e^{jt}} \rangle \right|^2 \right\}$

11: Update basis system:

12: $e_{\{a_2\}} \leftarrow \dfrac{\sqrt{1-|a_2|^2}}{1-\overline{a}_2 e^{jt}}$

13: $E_2 \leftarrow \dfrac{\sqrt{1-|a_2|^2}}{1-\overline{a}_2 e^{jt}} \cdot \dfrac{e^{jt}-a_1}{\sqrt{1-|a_1|^2}} E_1$

14: $N \leftarrow 2$

15: **While** $N < M$ **do**

16: Update residual component:

17: $G_{N+1} \leftarrow \left(G_N(t) - \langle G_N,\ e_{\{a_N\}}\rangle e_{\{a_N\}}\right) \dfrac{1-\overline{a}_N e^{jt}}{e^{jt}-a_N}$

18: Optimize parameter selection:

19: $a_{N+1} \leftarrow \underset{a_{N+1} \in D}{\arg\max} \left\{ \left| \langle G_{N+1}, \dfrac{\sqrt{1-|a_{N+1}|^2}}{1-\overline{a}_{N+1} e^{jt}} \rangle \right|^2 \right\}$

20: Update basis function:

21: $e_{\{a_{N+1}\}} \leftarrow \dfrac{\sqrt{1-|a_{N+1}|^2}}{1-\overline{a}_{N+1} e^{jt}}$

22: Update basis system:

23: $B_{N+1} \leftarrow \dfrac{\sqrt{1-|a_{N+1}|^2}}{1-\overline{a}_{N+1} e^{jt}} \cdot \dfrac{e^{jt}-a_N}{\sqrt{1-|a_N|^2}} B_N$

24: Increment counter:

25: $N \leftarrow N+1$

26: **end while**

2.3 *Experimental data*

The experimental data used in this article are sourced from the official information portal website of the Vietnamese Ministry of Health regarding the COVID-19 pandemic [39], spanning from January 23, 2020, when the first COVID-19 case was identified in Vietnam, to May 15, 2022, when Vietnam lifted its pandemic control measures. Vietnamese cities were selected as the study focus due to their comprehensive implementation of diverse, well-documented policy interventions that exhibited clear temporal separation between policy waves, enabling distinct analytical phases for intervention assessment. The consistent data reporting standards maintained across the study period ensured reliable longitudinal analysis, while the geographic and administrative diversity represented by cities such as Da Nang, a coastal tourism hub, and Hanoi, the national capital, provided opportunities for comparative policy effectiveness evaluation across different urban contexts and Vietnam's successful early pandemic response framework. Research conducted by Huynh et al. demonstrated that at the pandemic onset, 99.1% of hospital staff and 92.2% of the public possessed comprehensive understanding of COVID-19 [40, 41], indicating the government's proactive risk recognition and public awareness enhancement strategy that contributed to effective epidemic prevention measures.

The Vietnamese Ministry of Health officially divided the pandemic into four distinct waves based on different variants [42]: the original variant, D614G, Alpha, and Delta. Figure 1 shows the daily number of confirmed cases of COVID-19 in

Vietnam during the period of the epidemic studied here, during which the Vietnamese government established the steering committee on prevention and control of the epidemic to be responsible for the development of policies on prevention and control of the epidemic as a means of combating the spread of the epidemic. During the four waves of the epidemic, Vietnam developed a series of anti-epidemic policies, and the timely and precise policies controlled the spread of the epidemic.

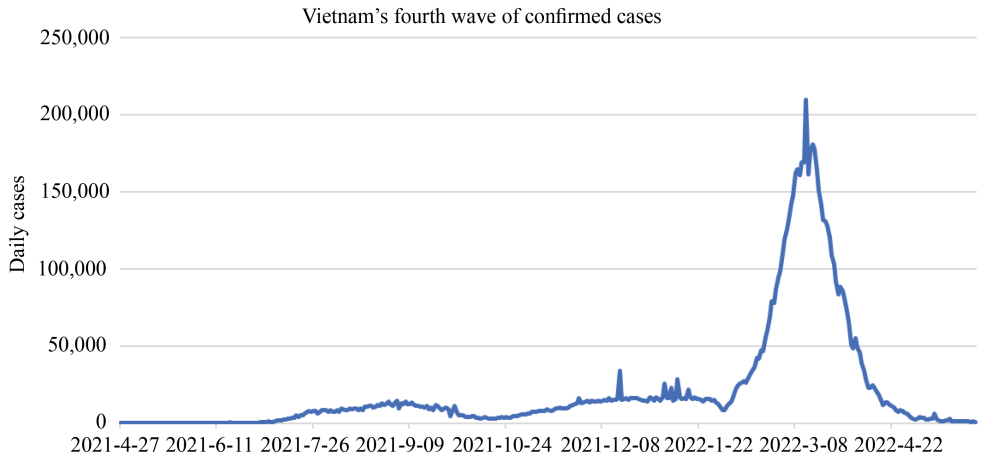

Figure 1. Daily infections of COVID-19 in Vietnam

2.4 *Pearson correlation coefficient*

The pearson correlation coefficient, usually denoted as 'r', is a statistical measure of the degree of linear correlation between two variables [43]. Pearson's coefficient is a unitless measure that depends only on the relative change in the data, not on the scale of the data. Its value ranges from -1 to 1, where -1 indicates a perfectly negative linear relationship, 1 indicates a perfectly positive linear relationship, and 0 indicates no linear relationship.

The pearson's correlation coefficient is calculated as:

$$r = \frac{\sum_{i=1}^{n}(x_i - \bar{x})(y_i - \bar{y})}{\sqrt{\sum_{i=1}^{n}(x_i - \bar{x})^2}\sqrt{\sum_{i=1}^{n}(y_i - \bar{y})^2}}, \tag{10}$$

Included among these:

(1) x_i and y_i are the observed values of the two variables, respectively.

(2) $\bar{x}$ and $\bar{y}$ are their mean values.

To apply the Pearson correlation coefficient in this study, we analyze the correlation between the decomposed components obtained from the AFD method and the original COVID-19 infection data. This analysis helps in understanding the relationship between the decomposed signal components and the actual epidemic trends, providing insights into the effectiveness of different policy measures.

By calculating the Pearson correlation coefficients for each decomposed component, we can identify which components have the strongest correlation with the original data. This allows us to determine the most significant factors influencing the epidemic trends and evaluate the impact of various anti-epidemic policies.

To summarize, the Pearson correlation coefficient is an essential tool in this study for quantifying the linear relationships between decomposed components and original infection data, thus providing a robust statistical foundation for analyzing the effectiveness of epidemic prevention measures.

3. Results and analysis

3.1 *Adaptive fourier decomposition component*

This section employs AFD to extract components under different time frequencies, examining the daily infection number changes of COVID-19 in Vietnam across various pandemic waves. In Figure 2, the components from the first to the eighth are vertically distributed according to frequency from low to high, reflecting the change in infection numbers at different frequencies, i.e., from overall to local changes. A to C represent different reconstruction methods from the first to third order.

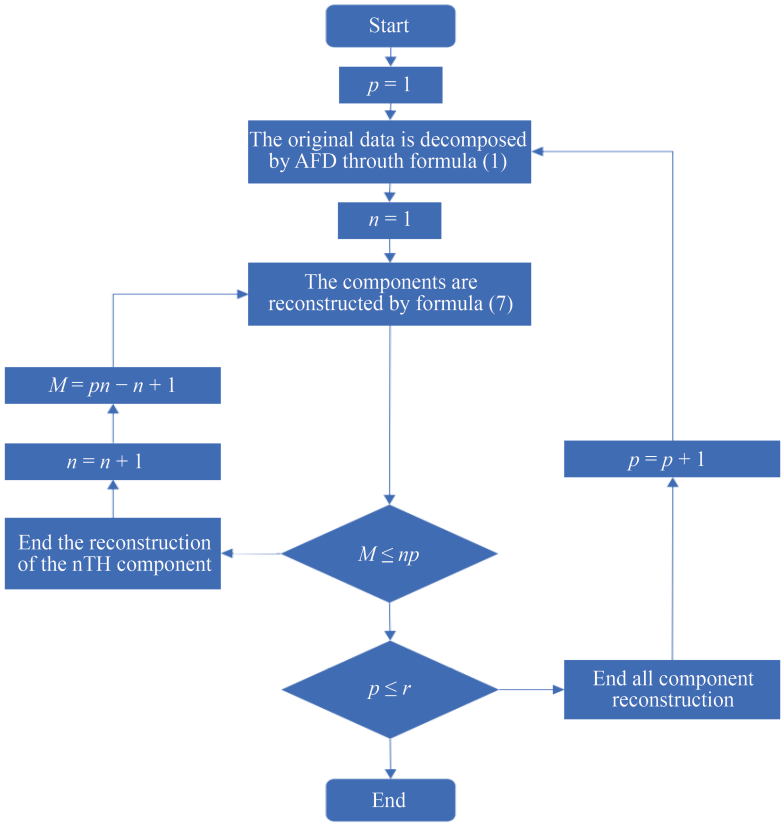

Figure 2. Signal decomposition flow chart

In Figure 3, Columns A, B, and C compare components from first-order, second-order, and third-order AFD decomposition, respectively. Examining the original daily infection numbers chart shows that the decomposition effects of the second and third orders are closer to the original data chart, better distinguishing the trend of infection numbers. This can preliminarily reflect the fluctuation of infection numbers under epidemic prevention measures during different periods. The component reconstruction of the third-order AFD better reflects the COVID-19 infection numbers under epidemic prevention policies. This pattern of higher-order decomposition (particularly third-order) offering superior trend resolution is further corroborated at the regional level: Figure 5 (Da Nang) and Figure 7 (Hanoi) demonstrate analogous results when decomposing their respective local infection data. The following discussion will explore the correlation between reconstructed components and changes in COVID-19 infection numbers under epidemic prevention policies and the correlation between different decomposition methods.

This study calculated the Pearson correlation coefficient for all decomposition results, as shown in Table 1. The correlation analysis was conducted within an interval with a p-value below 5%. Among different orders of AFD decomposition, the coefficient of the first component is significantly higher than the remaining components of the same

order, with the distribution decreasing sequentially from low to high frequency. The reconstruction results of the first-order, second-order, and third-order components are essentially the same, and the correlation values reflect the relationship between each element and the daily confirmed COVID-19 data. The strong correlation between components and the original data indicates that these components can better analyze fluctuations in the source data. As shown in Table 1, within the 5% significance level of correlation coefficients, except for the fifth and eighth components, all other components show a positive correlation trend with the original data.

Columns four to six of Table 1 present the correlation data for each order of AFD, all within 1%, indicating a strong correlation between the results of AFD decomposition. A comparison of multi-order decomposition results is provided in Table 3 for Da Nang and Table 5 for Hanoi. The coefficient of the first component in the third order is 0.994, the highest value compared to the other seven components; there is a negative correlation between the coefficient and frequency, meaning the coefficient decreases as the frequency increases.The superior performance of third-order AFD reconstruction stems from its optimal balance between signal fidelity and computational efficiency. The correlation coefficient of 0.994 for the first component indicates that third-order decomposition captures the primary trend while maintaining sensitivity to policy-induced fluctuations. The mathematical foundation lies in the adaptive Takenaka-Malmquist system, which adaptively selects optimal poles $\{a_m\}$ that minimize residual energy $\|G_{N+1}(e^{jt})\|^2$. Epidemiologically, third-order reconstruction captures: (1) primary epidemic trend (first component), (2) policy-induced oscillations (second component), and (3) variant-specific transmission patterns (third component) [44, 45].

Table 1. Correlation coefficient between the new component and the original infection data

	AFD-based	AFD-second	AFD-third	AFD-based & AFD-second	AFD-based & AFD-third	AFD-second & AFD-third
Comp.1	0.987***	0.991***	0.994***	0.996***	0.993***	0.998***
	(0.000)	(0.000)	(0.000)	(0.000)	(0.000)	(0.000)
Comp.2	0.091***	0.115***	0.129***	0.794***	0.708***	0.893***
	(0.007)	(0.001)	(0.000)	(0.000)	(0.000)	(0.000)
Comp.3	0.070**	0.091***	0.099***	0.770***	0.703***	0.913***
	(0.041)	(0.008)	(0.004)	(0.000)	(0.000)	(0.000)
Comp.4	0.058*	0.071**	0.076**	0.819***	0.765***	0.934***
	(0.089)	(0.038)	(0.026)	(0.000)	(0.000)	(0.000)
Comp.5	0.041	0.049	0.056	0.832***	0.726***	0.873***
	(0.235)	(0.153)	(0.102)	(0.000)	(0.000)	(0.000)
Comp.6	0.027	0.038	0.044	0.705***	0.623***	0.883***
	(0.426)	(0.260)	(0.202)	(0.000)	(0.000)	(0.000)
Comp.7	0.080**	0.075**	0.073**	0.940***	0.904***	0.962***
	(0.020)	(0.028)	(0.032)	(0.000)	(0.000)	(0.000)
Comp.8	0.015	0.015	0.012	1.000***	0.953***	0.953***
	(0.667)	(0.667)	(0.720)	(0.000)	(0.000)	(0.000)

Note: ***$p < 0.01$, **$p < 0.05$, *$p < 0.1$
The correlation coefficients are all estimated by Pearson's correlation method

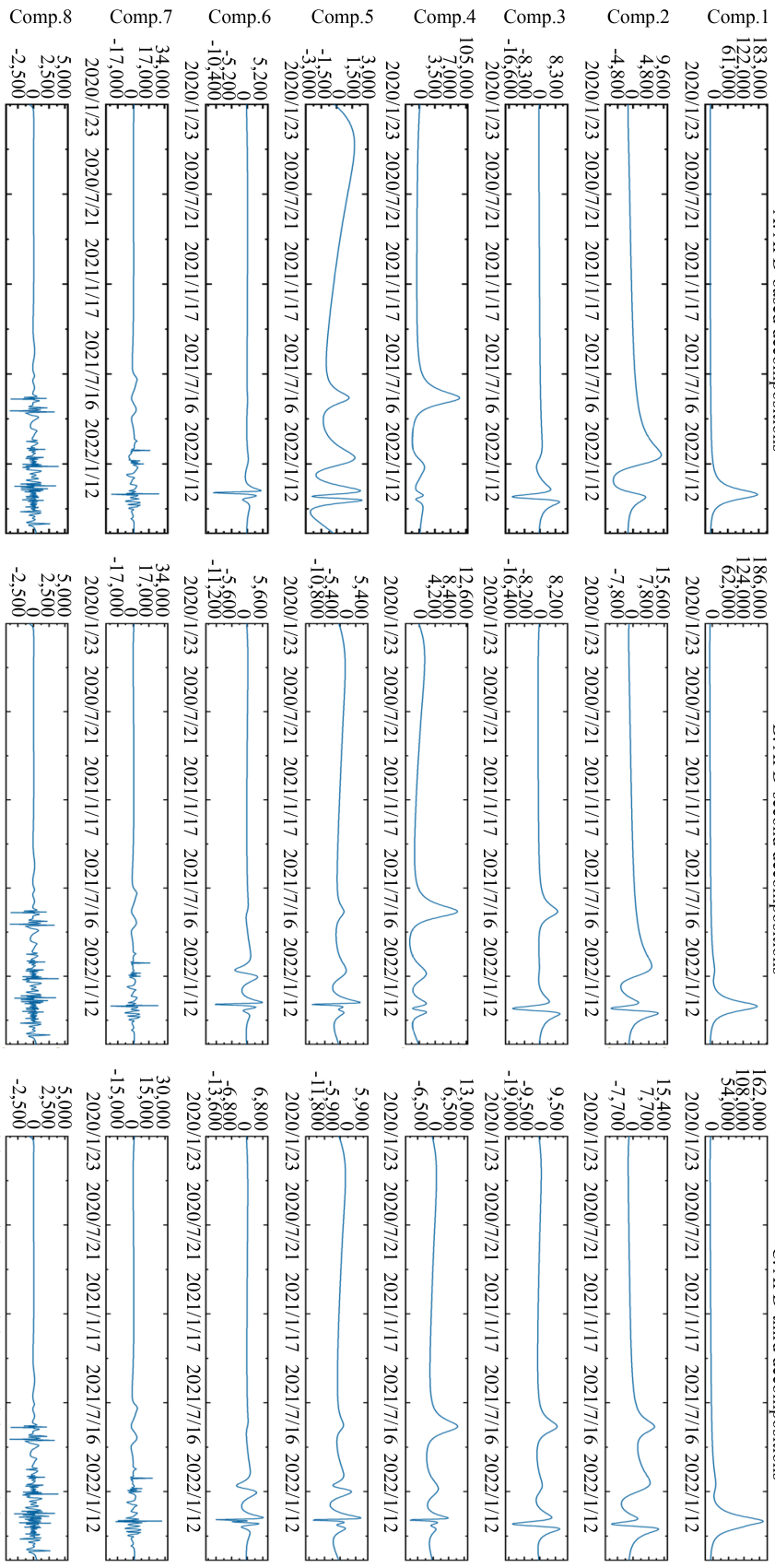

Figure 3. Better revealing trends in COVID-19 infection numbers: (a) AFD-based decompositions, (b) AFD-second decompositions, and (c) AFD-third decompositions

3.2 *Comparison of AFD with EMD and VMD*

Comparing common time-frequency decomposition methods (EMD, VMD) with AFD decomposition, their decomposition graphs are illustrated in Figure 4. The analysis results for each method in relation to the original data and the correlation results between methods are shown in Table 2. The first component coefficient of VMD is 0.841, significantly higher than the other components, and the coefficient decreases as the frequency increases, which is consistent with the AFD decomposition results.

Table 2 calculates the Pearson correlation coefficients among the decomposition results of AFD, EMD, and VMD to analyze the correlation between models. Under the premise of a 5% significance level, the components of AFD decomposition are generally positively correlated with EMD and VMD. In contrast, the correlation coefficients among other elements are insignificant, indicating a weak correlation between EMD and VMD. Figures 6 and 8 present comparative results between the AFD algorithm and other decomposition methods, respectively. The decomposition results demonstrate that AFD preserves richer peak feature details and exhibits superior decomposition performance compared to alternative algorithms. Tables 4 and 6 show the Pearson correlation coefficients between the original data and the decomposition results obtained by AFD, EMD, and VMD methods for Da Nang and Hanoi datasets, respectively. Statistical analysis reveals that AFD achieves significantly higher correlations with the original data compared to both EMD and VMD approaches. Therefore, AFD decomposition offers better reconstruction performance of the original data, enabling a more effective analysis of the efficacy of epidemic prevention policies.

Table 2. Correlation coefficient between the new component and the original infection data

	AFD-third	EMD	VMD	AFD-third & EMD	AFD-third & VMD	EMD & VMD
Comp.1	0.994***	0.548***	0.841***	0.557***	0.849***	0.171***
	(0.000)	(0.000)	(0.000)	(0.000)	(0.000)	(0.000)
Comp.2	0.129***	0.334***	0.718***	0.389***	0.093***	0.019
	(0.000)	(0.000)	(0.000)	(0.000)	(0.006)	(0.583)
Comp.3	0.099***	0.457***	0.057*	0.438***	0.013	0.010
	(0.004)	(0.000)	(0.093)	(0.000)	(0.707)	(0.764)
Comp.4	0.076**	0.620***	0.043	0.067**	0.048	0.010***
	(0.026)	(0.000)	(0.206)	(0.049)	(0.162)	(0.771)
Comp.5	0.056	0.513***	0.036	0.357***	0.049	0.007
	(0.102)	(0.000)	(0.288)	(0.000)	(0.152)	(0.833)
Comp.6	0.044	0.092***	0.034	0.119***	0.020	0.002
	(0.202)	(0.007)	(0.326)	(0.000)	(0.553)	(0.946)
Comp.7	0.073**	0.017	0.031	0.299***	0.350***	0.018
	(0.032)	(0.618)	(0.363)	(0.000)	(0.000)	(0.591)
Comp.8	0.012	0.161***	0.033	0.132***	0.201***	0.408***
	(0.720)	(0.000)	(0.338)	(0.000)	(0.000)	(0.000)

Note: ***$p < 0.01$, **$p < 0.05$, *$p < 0.1$
The correlation coefficients are all estimated by Pearson's correlation method

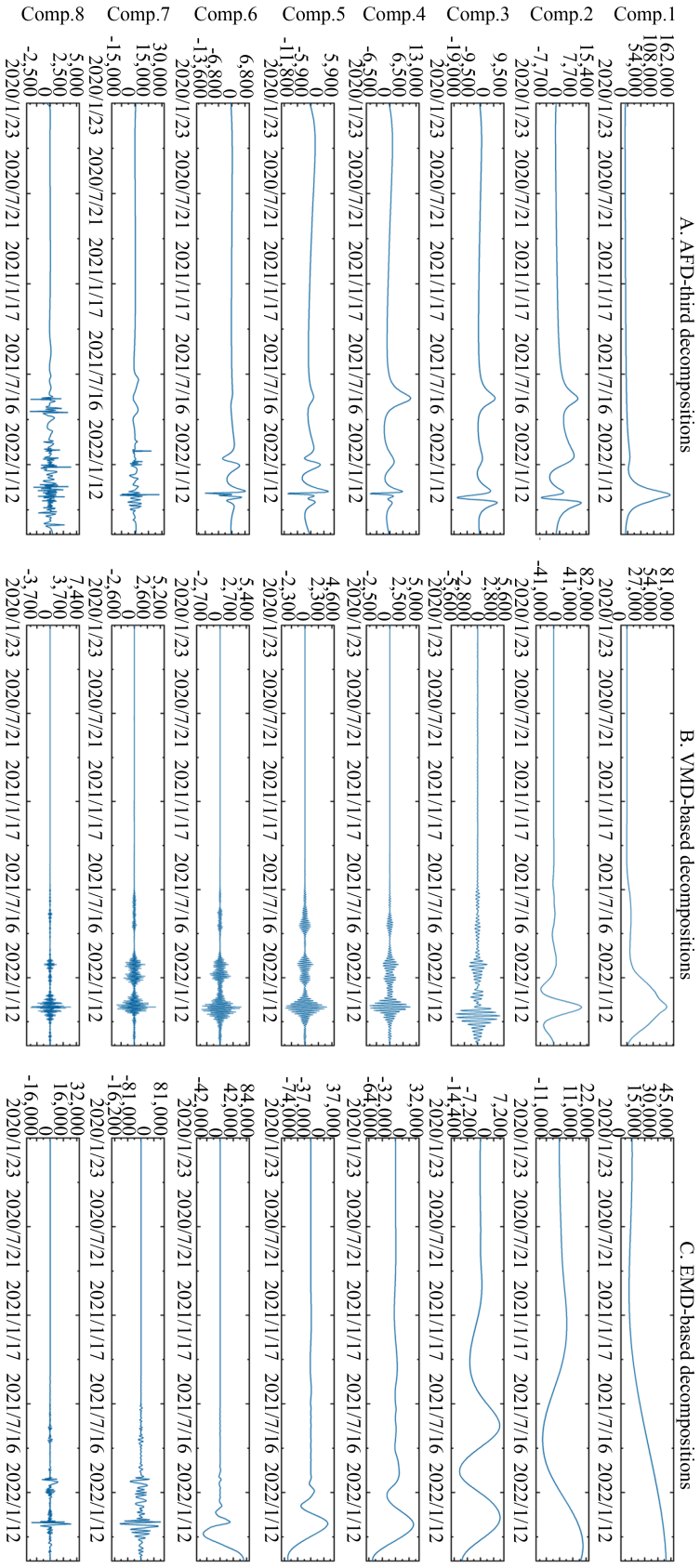

Figure 4. Correlation coefficients of AFD components with other algorithms: (a) AFD-third decompositions, (b) VMD-based decompositions, and (c) EMD-based decompositions

3.3 *AFD decomposition of COVID-19 infection data for different cities*

When analyzing the overall pandemic situation in Vietnam, we find that the effectiveness of policies is related to the city. The same policy implemented in different cities can have significantly different outcomes, making it necessary to analyze the infection data of cities in conjunction with the timing of policy implementation. This section will decompose Da Nang and Hanoi's daily COVID-19 infection data using AFD and conduct a correlation analysis using the Pearson correlation coefficient, discussing the decomposed data in conjunction with the previous data.

On July 25, 2020, Da Nang identified cases of the D614G strain, marking the beginning of the second wave of the pandemic. Da Nang announced social distancing measures on July 28, and the second wave of confirmed cases peaked at 45, followed by a general decline in total confirmed cases. By August 16, daily confirmed cases dropped to single digits; from August 31, there were no new confirmed cases. The second wave in Da Nang lasted for just over a month. The number of confirmed cases compared to the urban population and the swift implementation of social distancing measures effectively controlled the outbreak without causing widespread transmission. In Ho Chi Minh, services at non-essential places were immediately stopped on July 30 following the discovery of confirmed cases in Da Nang, with three confirmed cases appearing on July 31, and the number of new cases remained stable afterward. This trend resonates with the fifth component of the AFD decomposition. In contrast, the rapid changes in the sixth and seventh high-frequency components indicate that the social distancing measures significantly reduced the epidemic's energy release, quickly stabilizing the situation. This preliminary analysis suggests that the social distancing policies implemented in Da Nang were highly effective.

In Vietnam's first pandemic wave, Hanoi confirmed its first Covid-19 patient on March 4, 2020. On March 25, Hanoi announced an escalation in isolation measures and the shutdown of entertainment venues. The peak of this first wave came on March 30, with 13 cases confirmed in a single day. Afterward, the number of confirmed cases gradually declined, with no new cases reported after April 16. Ho Chi Minh announced the closure of non-essential service venues on March 15, and the number of confirmed cases peaked at eight on March 22. In Da Nang, after the announcement of social distancing controls during this wave, there were no significant numbers of confirmed cases, with the two confirmed cases imported from other provinces.

The third pandemic wave was marked by the discovery of two Alpha (B.1.1.7) cases in Vietnam. Due to its proximity to Quang Ninh Province, where the Alpha variant cases were confirmed, Hanoi halted public transportation to and from Quang Ninh on January 28. On January 31, Hanoi confirmed nine cases, the highest number during the third wave. Prompt transportation and infected individual isolation policies prevented a large-scale spread, and Hanoi began emergency vaccination. Ho Chi Minh locked down an apartment building with confirmed cases on February 6, with 29 cases confirmed on February 8. The number of confirmed cases then decreased to zero; the lockdown measures effectively cut off transmission routes, controlling the outbreak. Ho Chi Minh began promoting vaccination on March 9; Da Nang reported no local cases during the third wave.

The fourth wave was distinguished by the emergence of the Delta (B.1.617.2) variant. Between April 30 and May 3, 2021, Ho Chi Minh recorded its first case, implementing measures such as suspending the operation of entertainment venues and closing cinemas, which did not stop the spread of the pandemic. On May 31, the city began enforcing social distancing measures, extending them due to a rising trend in confirmed cases, indicating that these social distancing policies were not effectively controlling the outbreak. On August 23, the military took over pandemic control checkpoints, and on September 3, the daily confirmed cases numbered 8,499, with the number of cases decreasing daily.

Table 3. Coefficient of correlation between Da Nang new component and original data

	AFD-based	AFD-second	AFD-third	AFD-based & AFD-second	AFD-based & AFD-third	AFD-second & AFD-third
Comp.1	0.945***	0.972***	0.988***	0.973***	0.957***	0.983***
	(0.000)	(0.000)	(0.000)	(0.000)	(0.000)	(0.000)
Comp.2	0.225***	0.288***	0.295***	0.782***	0.763***	0.976***
	(0.000)	(0.000)	(0.000)	(0.000)	(0.006)	(0.583)
Comp.3	0.179***	0.191***	0.199*	0.942***	0.904	0.959
	(0.000)	(0.000)	(0.000)	(0.000)	(0.000)	(0.000)
Comp.4	0.064*	0.085**	0.102***	0.751***	0.628***	0.836***
	(0.061)	(0.013)	(0.003)	(0.000)	(0.000)	(0.000)
Comp.5	0.056	0.079**	0.094***	0.710***	0.599***	0.844
	(0.100)	(0.020)	(0.006)	(0.000)	(0.000)	(0.000)
Comp.6	0.056	0.075**	0.084**	0.742***	0.660***	0.890***
	(0.102)	(0.028)	(0.013)	(0.000)	(0.000)	(0.000)
Comp.7	0.107***	0.095***	0.086**	0.882***	0.803***	0.910***
	(0.002)	(0.006)	(0.012)	(0.000)	(0.000)	(0.591)
Comp.8	0.037	0.037	0.038	1.000***	0.984***	0.984***
	(0.665)	(0.667)	(0.720)	(0.000)	(0.000)	(0.000)

Note: ***$p < 0.01$, **$p < 0.05$, *$p < 0.1$
The correlation coefficients are all estimated by Pearson's correlation method

Table 4. Correlation of Da Nang AFD components with other algorithms

	AFD-third	EMD	VMD	AFD-third & EMD	AFD-third & VMD	EMD & VMD
Comp.1	0.988***	0.493***	0.945***	0.506***	0.944***	0.540***
	(0.000)	(0.000)	(0.000)	(0.000)	(0.000)	(0.000)
Comp.2	0.295***	0.533***	0.387***	0.068**	0.499***	0.012
	(0.000)	(0.000)	(0.000)	(0.045)	(0.000)	(0.736)
Comp.3	0.199***	0.709***	0.218***	−0.151***	0.639***	0.011
	(0.000)	(0.000)	(0.000)	(0.000)	(0.000)	(0.742)
Comp.4	0.102***	−0.128***	0.055	0.104***	0.040	0.003
	(0.003)	(0.000)	(0.104)	(0.002)	(0.243)	(0.920)
Comp.5	0.094***	0.301***	0.044	−0.008	0.010	0.003
	(0.006)	(0.000)	(0.202)	(0.804)	(0.768)	(0.930)
Comp.6	0.084**	0.065*	0.033	0.311***	0.017	0.008
	(0.013)	(0.058)	(0.334)	(0.000)	(0.611)	(0.805)
Comp.7	0.086**	0.103***	0.030	0.379***	0.070**	0.025
	(0.012)	(0.003)	(0.375)	(0.000)	(0.039)	(0.455)
Comp.8	0.038	0.022	0.030	0.483***	0.471***	0.451***
	(0.266)	(0.527)	(0.386)	(0.000)	(0.000)	(0.000)

Note: ***$p < 0.01$, **$p < 0.05$, *$p < 0.1$
The correlation coefficients are all estimated by Pearson's correlation method

Table 5. Coefficient of correlation between Hanoi new component and original data

	AFD-based	AFD-second	AFD-third	AFD-based & AFD-second	AFD-based & AFD-third	AFD-second & AFD-third
Comp.1	0.991***	0.995***	0.998***	0.996***	0.993***	0.997***
	(0.000)	(0.000)	(0.000)	(0.000)	(0.000)	(0.000)
Comp.2	0.089***	0.118***	0.123***	0.749***	0.721***	0.963***
	(0.009)	(0.001)	(0.000)	(0.045)	(0.000)	(0.736)
Comp.3	0.078**	0.085**	0.090***	0.921***	0.877***	0.952***
	(0.021)	(0.012)	(0.009)	(0.000)	(0.000)	(0.742)
Comp.4	0.033	0.043	0.047	0.771***	0.701***	0.909***
	(0.330)	(0.207)	(0.165)	(0.000)	(0.000)	(0.000)
Comp.5	0.052	0.045	0.040	0.851***	0.761***	0.894***
	(0.330)	(0.207)	(0.165)	(0.000)	(0.000)	(0.000)
Comp.6	0.007	0.007	0.007	1.000***	0.978***	0.978***
	(0.000)	(0.000)	(0.000)	(0.000)	(0.000)	(0.000)
Comp.7	0.991***	0.995***	0.998***	0.996***	0.993***	0.997***
	(0.000)	(0.000)	(0.000)	(0.000)	(0.000)	(0.000)
Comp.8	0.089***	0.118***	0.123***	0.749***	0.721***	0.963***
	(0.009)	(0.001)	(0.000)	(0.000)	(0.000)	(0.000)

Note: ***$p < 0.01$, **$p < 0.05$, *$p < 0.1$
The correlation coefficients are all estimated by Pearson's correlation method

Table 6. Correlation of Hanoi AFD components with other algorithms

	AFD-third	EMD	VMD	AFD-third & EMD	AFD-third & VMD	EMD & VMD
Comp.1	0.998***	0.586***	0.584***	0.596***	0.596***	0.299***
	(0.000)	(0.000)	(0.000)	(0.000)	(0.000)	(0.000)
Comp.2	0.123***	0.494***	0.663***	−0.247***	−0.188***	0.899***
	(0.000)	(0.000)	(0.000)	(0.000)	(0.000)	(0.000)
Comp.3	0.090***	0.330***	0.551***	0.044	0.311***	0.862***
	(0.009)	(0.000)	(0.000)	(0.199)	(0.000)	(0.000)
Comp.4	0.047	0.167***	0.332***	−0.046	−0.088**	0.778***
	(0.165)	(0.000)	(0.000)	(0.181)	(0.010)	(0.000)
Comp.5	0.040	0.057	0.025	0.038	0.342***	0.029
	(0.241)	(0.096)	(0.468)	(0.264)	(0.000)	(0.390)
Comp.6	0.007	0.067*	0.020	0.251***	0.070*	0.554***
	(0.829)	(0.049)	(0.561)	(0.000)	(0.040)	(0.000)
Comp.7	0.998***	0.586***	0.584***	0.596***	0.596***	0.299***
	(0.000)	(0.000)	(0.000)	(0.000)	(0.000)	(0.000)
Comp.8	0.123***	0.494***	0.663***	−0.247***	−0.188***	0.899***
	(0.000)	(0.000)	(0.000)	(0.000)	(0.000)	(0.000)

Note: ***$p < 0.01$, **$p < 0.05$, *$p < 0.1$
The correlation coefficients are all estimated by Pearson's correlation method

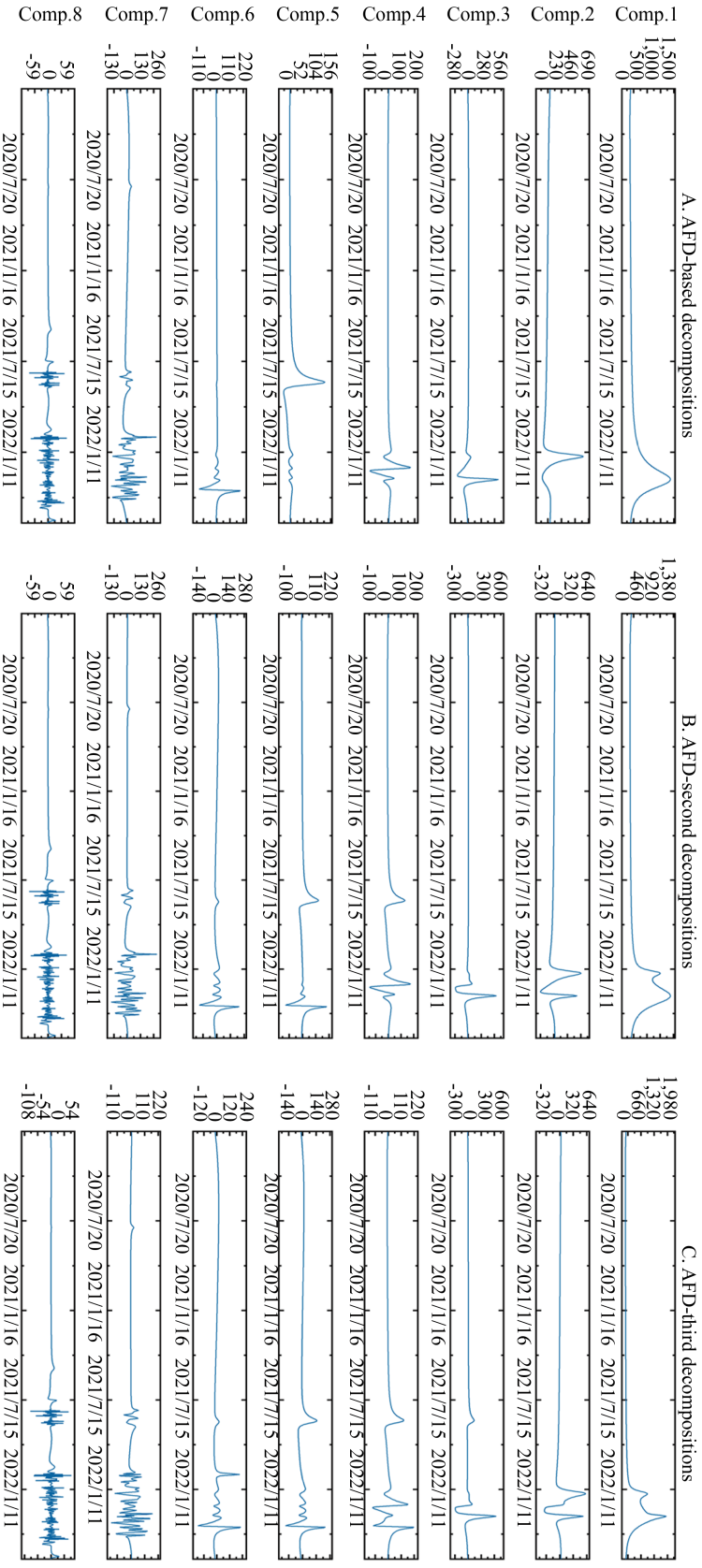

Figure 5. AFD components of Da Nang infection data: (a) AFD-based decompositions, (b) AFD-second decompositions, and (c) AFD-third decompositions

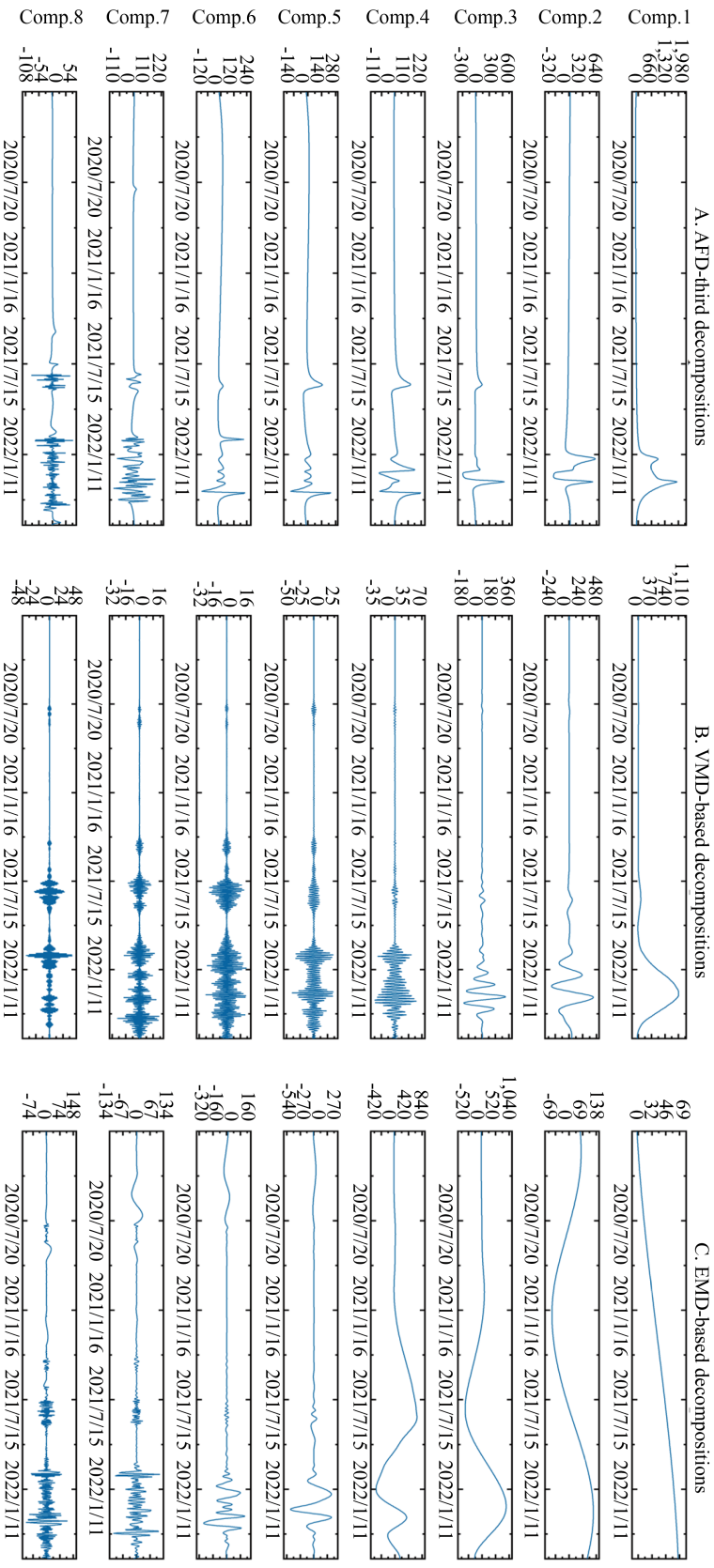

Figure 6. Da Nang infection data decomposition by different algorithms: (a) AFD-third decompositions, (b) VMD-based decompositions, and (c) EMD-based decompositions

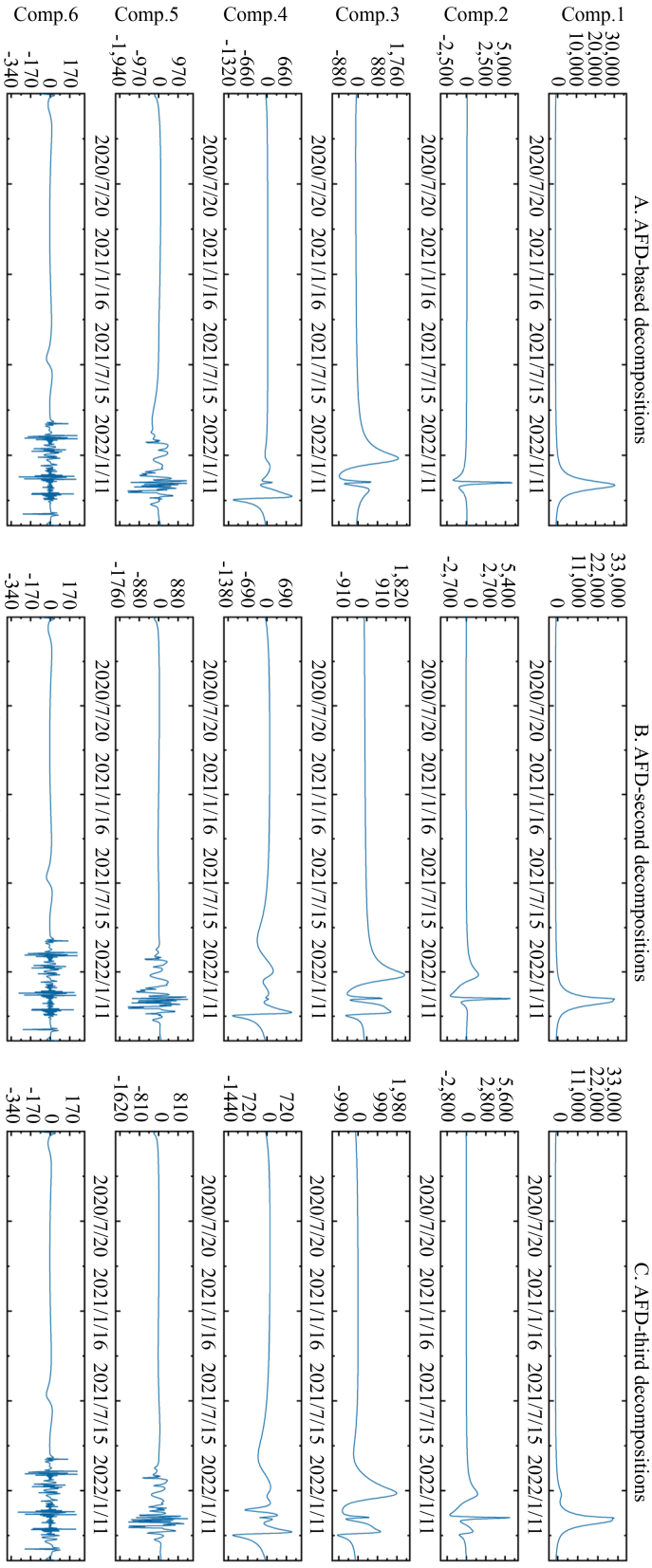

Figure 7. AFD components of Hanoi infection data: (a) AFD-based decompositions, (b) AFD-second decompositions, and (c) AFD-third decompositions

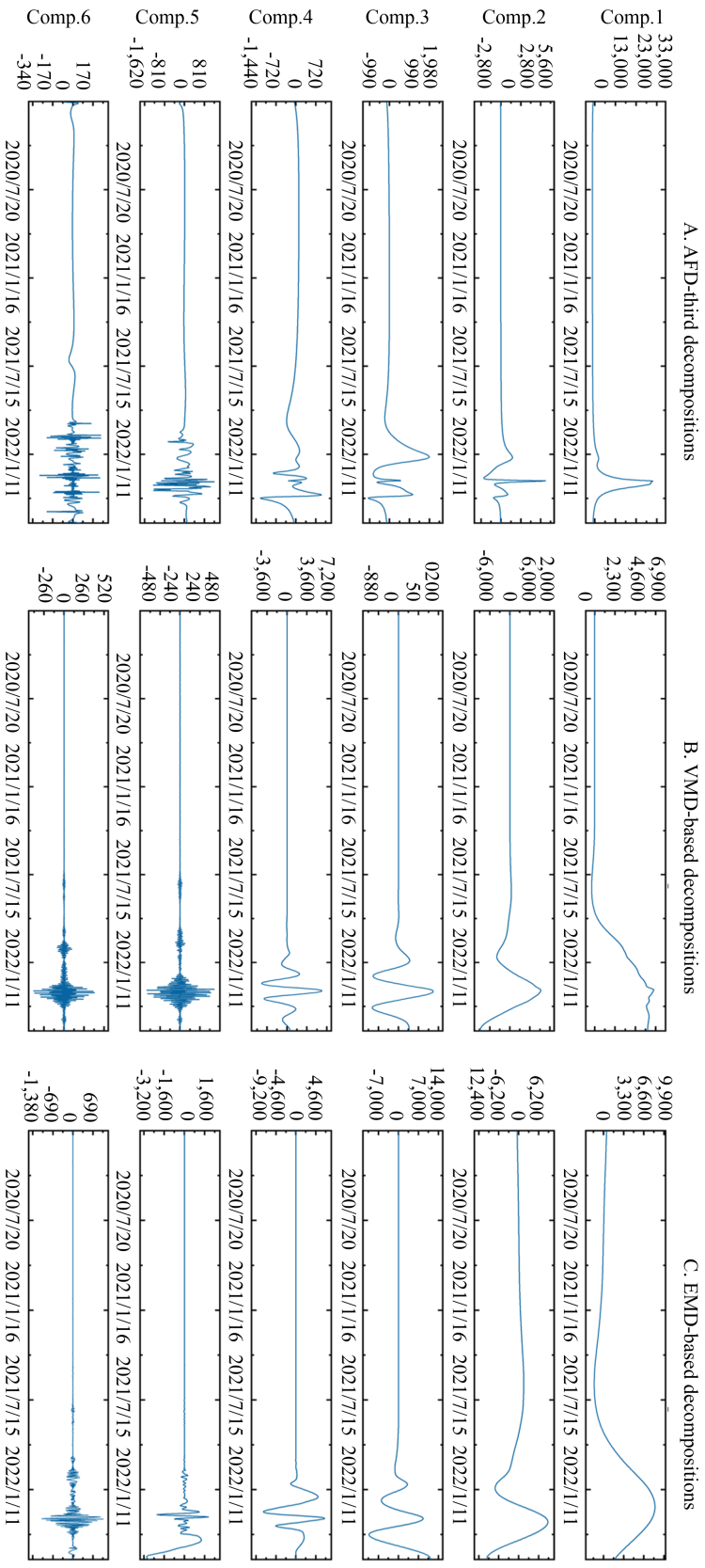

Figure 8. Hanoi infection data decomposition by different algorithms: (a) AFD-third decompositions, (b) VMD-based decompositions, and (c) EMD-based decompositions

4. Discussion

Combining the data from the second wave of the pandemic in Da Nang and analyzing the changes in infection data during the implementation of the AFD decomposition policy, Figure 9 demonstrates the effectiveness of closing non-essential businesses in both Ho Chi Minh City and Hanoi. During the early stages of the first wave, this policy was sustained for 15 days in Ho Chi Minh and 28 days in Hanoi, with daily confirmed cases decreasing from the peak to zero. This reflects the precise and practical nature of Vietnam's initial pandemic response policies. Regarding social distancing policies, Da Nang and Hanoi's prevention and control measures served as exemplary models. Da Nang's second wave lasted for 40 days, during which the number of confirmed cases dropped from a daily high of 45 to zero over 35 days. Following the implementation of social distancing policies, the overall trend of confirmed cases showed a significant decline, marking it as the most effective pandemic prevention effort; Hanoi also promptly adopted isolation measures during its second wave, preventing the spread of the virus within the city and underscoring the importance of isolation policies.

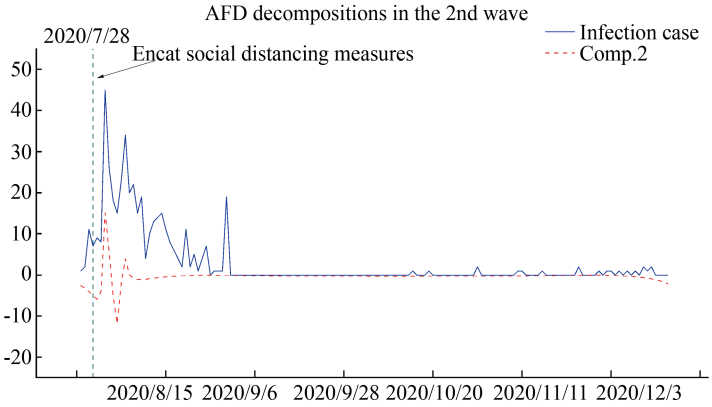

Figure 9. AFD decomposition of the second wave of the epidemic in Da Nang

Analysis presented in Figure 10 reveals a distinct shift in epidemic wave characteristics following increased vaccination: peaks occurring before vaccination demonstrated stronger intensity and longer duration, whereas those emerging after significant vaccination uptake showed substantially diminished intensity and shorter duration.

In terms of vaccine policy, Vietnam acquired a large number of vaccines internationally through the Vaccine Foundation. It began a widespread vaccination campaign on July 1, 2021, marking the start of its vaccine strategy. Before the mass promotion of vaccines during the fourth wave, the proportion of the population in Vietnam that had received the first dose of the COVID-19 vaccine was 67.2%, and only 6.4% had received the second dose. At this time, the daily average number of confirmed cases in Ho Chi Minh gradually increased, with a peak of 8,499 cases. By November 30, the vaccination data showed a first-dose coverage rate of 99.4% and a second-dose coverage rate of 89.9%. At this point, the number of confirmed cases in Ho Chi Minh had dropped to fewer than a thousand daily cases. This demonstrates that as the vaccination coverage rate increased, the number of confirmed cases in Ho Chi Minh gradually decreased. However, the vaccination process requires time.

In this study, the daily data and various epidemic prevention measures of the four pandemic waves in Vietnam were carefully examined, and the epidemic data were dissected using AFD and analyzed for correlation with the original data using the Pearson correlation coefficient. By integrating the anti-epidemic policies implemented by the government, it was found that some of the policies resonated with the high-frequency components of the decomposition results, some of them resonated with the low-frequency components of the decomposition results, and some of them were weakly correlated with the decomposition results, which was closely related to the effectiveness of the policy implementation. The policy of maintaining social distance proved to be very effective in rapidly controlling the pandemic in a short period without

expanding the infected area, which correlates with the sixth and seventh components of the decomposition of the Da Nang data. However, in Wave 4, the social distance policy in Ho Chi Minh was no longer correlated with the results of the AFD decomposition, suggesting that the policy gradually lost its effectiveness in the later stages of the pandemic due to the increased infectiousness of the mutated strains. The vaccination policy introduced in Ho Chi Minh added a new dimension to the effectiveness of pandemic prevention. By the late fourth wave, when vaccination rates reached a certain percentage, the policy of receiving two vaccine doses was associated with the third component of the AFD decomposition results. This suggests that the vaccination policy effectively reduced daily COVID-19 infection data, although its effectiveness may have been reduced due to the ability of the viral strain to evade immunization.

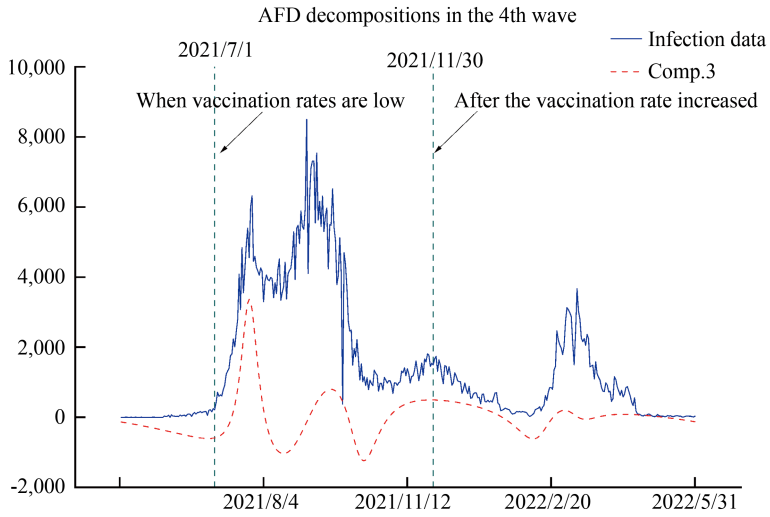

Figure 10. AFD decomposition of the fourth wave of the epidemic in Ho Chi Minh

While our analysis demonstrates strong correlations between domestic policies and infection dynamics (correlation coefficient of 0.994 for the primary AFD component), we acknowledge that Vietnam's epidemic response occurred within a broader international context. Several factors support our domestic-focused analytical approach.

Vietnam's early implementation of comprehensive international travel restrictions and border controls effectively minimized external policy spillover effects during critical epidemic phases. The country's proactive border management created conditions more isolated than typical international scenarios. The high-frequency components (sixth and seventh) in our AFD decomposition show rapid policy-induced changes that align temporally with domestic interventions rather than international policy announcements, suggesting domestic policies were the primary drivers of observed frequency patterns.The AFD methodology's ability to capture policy-induced frequency changes demonstrates particular sensitivity to domestic interventions, as evidenced by the strong correlation between policy implementation timing and component oscillations. Nevertheless, future research could benefit from multi-country comparative AFD analysis to examine cross-border policy interdependencies, particularly for countries with more porous borders or greater international integration.

5. Conclusions

This study employs AFD methodology to comprehensively analyze COVID-19 infection rate dynamics under policy interventions, using Vietnam as a case study. Our approach innovatively integrates multidimensional analytical metrics to elucidate epidemic influencing factors across temporal scales. Results demonstrate that non-essential business closures proved effective in Ho Chi Minh City and Hanoi, while social distancing policies and vaccination measures generated two distinct periods of infection fluctuation with temporally differentiated impacts. Multiscale analysis revealed

positive proportionality between AFD component frequencies of daily new infections and Pearson correlation coefficients, indicating strong interdependence that shifted from high-frequency to low-frequency components as pandemic prevention policies continued implementation, suggesting diminishing policy effectiveness over time. AFD exhibits distinct methodological advantages over EMD and VMD approaches through its foundation in complex Hardy space theory, providing robust theoretical guarantees for signal decomposition while demonstrating superior boundary effect resistance crucial for finite epidemic datasets. The method's adaptive parameter selection via maximum projection principle eliminates manual tuning requirements inherent in VMD applications. These findings suggest significant implications for epidemic preparedness: multiscale monitoring systems can leverage AFD-based frameworks for systematic policy effectiveness evaluation across temporal scales, while real-time assessment capabilities enable rapid intervention impact evaluation and early warning system development through frequency domain insights for trend prediction and optimal policy timing.

Acknowledgement

Great appreciation is extended to Lu for providing valuable insights during the writing process and for the meticulous review of the manuscript. Constructive comments and insightful suggestions from the anonymous reviewers are also gratefully acknowledged, which have significantly improved the quality of the manuscript.This research was supported by the Science and Technology Development Fund of Macau SAR (Grant No. 0002/2024/RDP) and the National Key Research and Development Program of China (Grant No. 2024YFE0214800).

Data availability

Data from the official website of the Ministry of Health of Vietnam https://Covid-19.gov.vn/.

Conflict of interest

The authors declare no competing financial interest.

References

[1] Xiang Y, Jia Y, Chen L, Guo L, Shu , Long E. COVID-19 epidemic prediction and the impact of public health interventions: A review of COVID-19 epidemic models. *Infectious Disease Modelling*. 2021; 6: 324-342. Available from: https://doi.org/10.1016/j.idm.2021.01.001.

[2] Nguyen TV, Dai Tran Q, Phan LT, Vu LN, Truong DTT, Truong HC, et al. In the interest of public safety: rapid response to the COVID-19 epidemic in Vietnam. *BMJ Global Health*. 2021; 6: e004100. Available from: https://doi.org/10.1136/bmjgh-2020-004100.

[3] Wu Y, Zhang Q, Li L, Li M, Zuo Y. Control and prevention of the COVID-19 epidemic in China: a qualitative community case study. *Risk Management and Healthcare Policy*. 2021; 2021(14): 4907-4922. Available from: https://doi.org/10.2147/RMHP.S336039.

[4] Hon C, Liu Z, Qian , Qu W, Zhao J. Trends by adaptive Fourier decomposition and application in prediction. *International Journal of Wavelets, Multiresolution and Information Processing*. 2024; 22(5): 2450014. Available from: https://doi.org/10.1142/S0219691324500140.

[5] Hoang VM, Hoang HH, Khuong QL, La NQ, Tran TTH. Describing the pattern of the COVID-19 epidemic in Vietnam. *Global Health Action*. 2020; 13: 1776526. Available from: https://doi.org/10.1080/16549716.2020.1776526.

[6] Jin K, Tang X, Qian Z, Wu Z, Yang Z, Qian T, Hon C, Lu J. Modeling viral evolution: A novel SIRSVIDE framework with application to SARS-CoV-2 dynamics. *hLife*. 2024; 2: 227-245. Available from: https://doi.org/10.1016/j.hlife.2024.03.006.

[7] Liang J, Wang Y, Lin Z, He W, Sun J, Li Q, et al. Influenza and COVID-19 co-infection and vaccine effectiveness against severe cases: a mathematical modeling study. *Frontiers in Cellular and Infection Microbiology*. 2024; 14: 1347710. Available from: https://doi.org/10.3389/fcimb.2024.1347710.

[8] Wang Y, Yang C, Liu Y, Zhang J, Qu W, Liang J, et al. Seroprevalence of avian influenza A (H5N6) virus infection, Guangdong province, China, 2022. *Emerging Infectious Diseases*. 2024; 30: 826. Available from: https://doi.org/10.3201/eid3004.231226.

[9] Kermack WO, McKendrick AG. A contribution to the mathematical theory of epidemics. *Proceedings of the Royal Society of London. Series A, Containing Papers of a Mathematical and Physical Character*. 1927; 115: 700-721. Available from: https://doi.org/10.1098/rspa.1927.0118.

[10] Soebiyanto RP, Adimi F, Kiang RK. Modeling and predicting seasonal influenza transmission in warm regions using climatological parameters. *PLoS ONE*. 2010; 5: e9450. Available from: https://doi.org/10.1371/journal.pone.0009450.

[11] Gani J. Modelling epidemic diseases. *Australian & New Zealand Journal of Statistics*. 2010; 52: 321-329. Available from: https://doi.org/10.1111/j.1467-842X.2010.00586_1.x.

[12] Esquível ML, Krasii NP, Guerreiro GR, Patrício P. The multi-compartment SI (RD) model with regime switching: An application to COVID-19 pandemic. *Symmetry*. 2021; 13: 2427. Available from: https://doi.org/10.3390/sym13122427.

[13] You G, Gan S, Guo H, Dagestani AA. Public opinion spread and guidance strategy under COVID-19: a SIS model analysis. *Axioms*. 2022; 11: 296. Available from: https://doi.org/10.3390/axioms11060296.

[14] Alenezi MN, Al-Anzi FS, Alabdulrazzaq H. Building a sensible SIR estimation model for COVID-19 outspread in Kuwait. *Alexandria Engineering Journal*. 2021; 60: 3161-3175. Available from: https://doi.org/10.1016/j.aej.2021.01.025.

[15] Tsvetkov V, Mikheev S, Tsvetkov I, Derbov V, Gusev A, Vinitsky S. Modeling the multifractal dynamics of COVID-19 pandemic. *Chaos, Solitons & Fractals*. 2022; 161: 112301. Available from: https://doi.org/10.1016/j.chaos.2022.112301.

[16] Saha S, Dutta P, Samanta G. Dynamical behavior of SIRS model incorporating government action and public response in presence of deterministic and fluctuating environments. *Chaos, Solitons & Fractals*. 2022; 164: 112643. Available from: https://doi.org/10.1016/j.chaos.2022.112643.

[17] Hamzah FB, Lau C, Nazri H, Ligot DV, Lee G, Tan CL, et al. CoronaTracker: worldwide COVID-19 outbreak data analysis and prediction. *Bull World Health Organ*. 2020; 1: 1-32. Available from: https://doi.org/10.2471/BLT.20.255695.

[18] Basnarkov L. SEAIR Epidemic spreading model of COVID-19. *Chaos, Solitons & Fractals*. 2021; 142: 110394. Available from: https://doi.org/10.1016/j.chaos.2020.110394.

[19] Qian T, Wang J, Mai W. An enhancement algorithm for cyclic adaptive Fourier decomposition. *Applied and Computational Harmonic Analysis*. 2019; 47: 516-525. Available from: https://doi.org/10.1016/j.acha.2019.01.003.

[20] Qian T, Zhang Y, Liu W, Qu W. Adaptive Fourier decomposition-type sparse representations versus the Karhunen-Loève expansion for decomposing stochastic processes. *Mathematical Methods in the Applied Sciences*. 2023; 46: 14007-14025. Available from: https://doi.org/10.1002/mma.9301.

[21] Dong R, Ni S, Ikuno S. Nonlinear frequency analysis of COVID-19 spread in Tokyo using empirical mode decomposition. *Scientific Reports*. 2022; 12: 2175. Available from: https://doi.org/10.1038/s41598-022-06095-w.

[22] Qian T, Zhang L, Li Z. Algorithm of adaptive Fourier decomposition. *IEEE Transactions on Signal Processing*. 2011; 59: 5899-5906. Available from: https://doi.org/10.1109/TSP.2011.2168520.

[23] Li X, He H, Huang J, Liu R, Qian T, Hon C. ASFM-AFD: Multimodal Fusion of AFD-Optimized LiDAR and Camera Data for Paper Defect Detection. *IEEE Transactions on Instrumentation and Measurement*. 2025; 74: 3545514. Available from: https://doi.org/10.1109/TIM.2025.3580902.

[24] Li X, Lin Y, He W, Liu R, Oliveira AL, Qian T, et al. Enhancing the interpretation of spirometry: joint utilization of n-order adaptive fourier decomposition and deep learning techniques. *IEEE Transactions on Instrumentation and Measurement*. 2025; 74: 5026514. Available from: https://doi.org/10.1109/TIM.2025.3557112.

[25] Qian T. Sparse representations of random signals. *Mathematical Methods in the Applied Sciences*. 2022; 45: 4210-4230. Available from: https://doi.org/10.1002/mma.8033.

[26] Qian T, Wang YB. Adaptive Fourier series-a variation of greedy algorithm. *Advances in Computational Mathematics*. 2011; 34: 279. Available from: https://doi.org/10.1007/s10444-010-9153-4.

[27] Tao Q, Yan BW, Pei D. Adaptive decomposition into mono-components. *Advances in Adaptive Data Analysis*. 2009; 1(4): 703−709. Available from: https://doi.org/10.1142/S1793536909000278.

[28] Wang Z, Wong CM, Rosa A, Qian T, Wan F. Adaptive Fourier decomposition for multi-channel signal analysis. *IEEE Transactions on Signal Processing*. 2022; 70: 903-918. Available from: https://doi.org/10.1109/TSP.2022.3143723.

[29] Wang Z, Wan F, Wong CM. Fast basis search for adaptive Fourier decomposition. *EURASIP Journal on Advances in Signal Processing*. 2018; 2018(74). Available from: https://doi.org/10.1186/s13634-018-0593-1.

[30] Wang Z, Wan F, Wong CM, Zhang L. Adaptive Fourier decomposition based ECG denoising. *Computers in Biology and Medicine*. 2016; 77: 195-205. Available from: https://doi.org/10.1016/j.compbiomed.2016.08.013.

[31] Tao Q, Wang Y. Remarks on adaptive Fourier decomposition. *International Journal of Wavelets, Multiresolution and Information Processing*. 2013; 11(1): 1350007. Available from: https://doi.org/10.1142/S0219691313500070.

[32] Tartof SY, Slezak JM, Fischer H, Hong V, Ackerson BK, Ranasinghe ON, et al. Effectiveness of mRNA BNT162b2 COVID-19 vaccine up to 6 months in a large integrated health system in the USA: a retrospective cohort study. *The Lancet*. 2021; 398: 1407-1416. Available from: https://doi.org/10.1016/S0140-6736(21)02183-8.

[33] Duren PL. *Theory of H^p Spaces*. New York: Academic Press; 1970.

[34] Mo Y, Qian T, Mai W, Chen Q. The AFD methods to compute Hilbert transform. *Applied Mathematics Letters*. 2015; 45: 18-24. Available from: https://doi.org/10.1016/j.aml.2014.12.017.

[35] Qian T. Cyclic AFD algorithm for the best rational approximation. *Mathematical Methods in the Applied Sciences*. 2014; 37: 846-859. Available from: https://doi.org/10.1002/mma.2843.

[36] Qian T. Intrinsic mono-component decomposition of functions: an advance of Fourier theory. *Mathematical Methods in the Applied Sciences*. 2010; 33: 880-891. Available from: https://doi.org/10.1002/mma.1214.

[37] Qu W, Chui CK, Deng GT, Qian T. Sparse representation of approximation to identity. *Analysis and Applications*. 2022; 20: 815-837. Available from: https://doi.org/10.1142/S0219530521500251.

[38] Qu W, Qian T, Deng GT. A stochastic sparse representation: *n*-best approximation to random signals and computation. *Applied and Computational Harmonic Analysis*. 2021; 55: 185-198. Available from: https://doi.org/10.1016/j.acha.2021.05.003.

[39] Ban Chỉ đạo Quốc gia phòng chống dịch COVID-19 [National Steering Committee for COVID-19 Prevention and Control]. Available from: https://Covid-19.gov.vn/ [Accessed 1st April 2021].

[40] Huynh G, Nguyen TV, Nguyen DD, Lam QM, Pham TN, Nguyen HTN. Knowledge about COVID-19, beliefs and vaccination acceptance against COVID-19 among high-risk people in Ho Chi Minh City, Vietnam. *Infection and Drug Resistance*. 2021; 14: 1773-1780. Available from: https://doi.org/10.2147/IDR.S308446.

[41] Huynh G, Han NTN, Ngan VK, Van Tam V, Le An P. Knowledge and attitude toward COVID-19 among healthcare workers at District 2 Hospital, Ho Chi Minh City. *Asian Pacific Journal of Tropical Medicine*. 2020; 13: 260-265. Available from: https://doi.org/10.1101/2020.04.27.20081859.

[42] Huong G. *VietNam's two-year fight against COVID-19*. Government News of the Socialist Republic of Vietnam; 2022. Available from: https://en.baochinhphu.vn/viet-nams-two-year-fight-against-covid-19-1122012315045993.htm [Accessed 23th January 2022].

[43] Saccenti E, Hendriks MH, Smilde AK. Corruption of the Pearson correlation coefficient by measurement error and its estimation, bias, and correction under different error models. *Scientific Reports*. 2020; 10: 438. Available from: https://doi.org/10.1038/s41598-019-57247-4.

[44] Hethcote HW. The mathematics of infectious diseases. *Siam Review*. 2000; 42(4): 599-653. Available from: https://doi.org/10.1137/S0036144500371907.

[45] Diekmann O, Heesterbeek JAP, Metz JA. On the definition and the computation of the basic reproduction ratio R0 in models for infectious diseases in heterogeneous populations. *Journal of Mathematical Biology*. 1990; 28: 365-382. Available from: https://doi.org/10.1007/BF00178324.